THE JOURNAL OF PHYSICAL CHEMISTRY B

Article

pubs.acs.org/JPCB

# Measurement of Proton Chemical Shifts in Invisible States of Slowly Exchanging Protein Systems by Chemical Exchange Saturation Transfer

Guillaume Bouvignies*,† and Lewis E. Kay*,†,‡

†Departments of Molecular Genetics, Biochemistry and Chemistry, The University of Toronto, Toronto, Ontario, Canada, M5S 1A8

‡Program in Molecular Structure and Function, Hospital for Sick Children, 555 University Avenue, Toronto, Ontario, Canada, M5G 1X8

Supporting Information

**ABSTRACT:** Chemical exchange saturation transfer (CEST) NMR spectroscopy has emerged as a powerful technique for studies of transiently formed, sparsely populated (excited) conformational states of protein molecules in slow exchange with a dominant structure. The most popular form of the experiment, and the version originally developed, uses a weak $^{1}H$ radio frequency field to perturb longitudinal magnetization of one state with the effect transferred to magnetization in the second conformation via chemical exchange. A significant limitation of the method for protein applications emerges from $^{1}H$ magnetization transfer via dipolar relaxation (NOE effect) that can severely complicate analysis of the resulting CEST profile. This is particularly an issue since the $^{1}H$ chemical shifts of the excited state, critical for structural studies of these elusive conformers, become difficult to extract. Here we present a method for measurement of these shifts via CEST experiments in which the NOE effect is not an issue. The methodology is illustrated through applications to a pair of exchanging systems where the results are cross-validated.

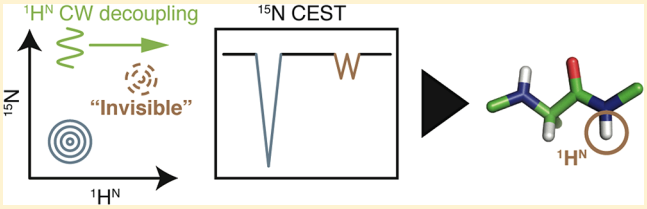


## INTRODUCTION

Biomolecular function is often dictated by excursions between different molecular conformations.[1] While detailed studies of the most prevalent (ground state) structures are often possible, corresponding studies of sparsely populated conformers are not as common since the biophysical tools amenable to their investigation are less developed. However, over the past decade significant advances have been made in relaxation dispersion NMR spectroscopy,[2,3] increasing its utility as a method for studying sparsely populated and transiently formed conformations of proteins[4−9] and nucleic acids.[10,11] For exchange processes ranging between approximately 200 and 2000 $s^{-1}$ the Carr−Purcell−Meiboom−Gill (CPMG) approach,[12,13] conceived over five decades ago, remains widely used because measured relaxation dispersion profiles depend on exchange rates (kinetics), fractional populations of exchanging states (thermodynamics) and differences in chemical shifts, $\Delta\varpi$ (ppm), between interconverting states that can be robustly extracted from fits of the experimental data. Values of $\Delta\varpi$ are critical for structural studies of sparsely populated conformers (referred to in what follows as conformationally excited states) because chemical shifts can be related to structure.[14,15] For rates of exchange that are less than approximately 100−200 $s^{-1}$ and where excited state(s) are not visible in spectra it can be difficult to extract correct estimates of exchange parameters and chemical shift differences from CPMG data.[16] In this regime, CEST-based experiments become powerful.[17] Here a series of spectra are recorded as a function of the position of a weak radio frequency field. When the applied field is proximal to a peak derived from one of a pair of exchanging states, the sparsely populated conformer for example, the effect of the perturbation extends to the peak from the second (ground) state, facilitating the extraction of exchange rates and chemical shifts of the excited state conformer.[16,18−20] Note that in general such shifts are not available from standard NMR spectra because the excited state is "invisible".

Initial protein applications of this methodology include the work of Gupta and Redfield[19] and, subsequently, Roberts, Fenney, and co-workers,[18,21] where the methodology was used to assign resonances from one conformation based on known assignments of a second state and to obtain the kinetics of the exchange process. Balaban and co-workers[22] and then van Zijl et al.[23] subsequently showed that it is possible to image via saturation transfer from a reporter molecule to water, thereby amplifying the signal many fold. In an important application to studies of exchange in protein systems, Fawzi et al. measured magnetization transfer from $^{15}N$ to quantify both the interconversion of A$\beta$ between free peptide and high molecular weight protofibrils and the $^{15}N$ linewidths of the invisible fibril state resonances.[20] Building on these ideas, our laboratory has developed and applied $^{15}N$[16] and $^{13}C$[24] CEST schemes for extracting exchange parameters and $\Delta\varpi$ values in exchanging protein systems with exchange rates on the order of 100 $s^{-1}$ and where the excited state is not observed in NMR spectra. Herein we extend this methodology to studies involving the measure-

Received: November 9, 2012
Published: November 29, 2012

   dx.doi.org/10.1021/jp311109u | J. Phys. Chem. B 2012, 116, 14311−14317

ment of $^1$H $\Delta\varpi$ values in proteins undergoing slow chemical exchange using a novel CEST experiment that circumvents limitations to $^1$H applications that have been problematic in the past. The utility of the methodology is illustrated with examples involving (i) the folding of an A39G mutant of a small four helix bundle protein and (ii) the interconversion of the L99A cavity mutant of T4 lysozyme between a pair of distinct conformational states.

## MATERIALS AND METHODS

**Sample Preparation.** Protein L was expressed and purified as described previously.[25] The sample concentration was 4 mM [U−$^{15}$N,$^2$H]-labeled protein dissolved in 50 mM sodium phosphate, 0.05% $NaN_3$, 10% $D_2O$ buffer (pH 6.0). A [U−$^{15}$N]-labeled A39G FF domain sample was prepared as described by Fersht and co-workers.[26] The sample used was 2 mM in protein, 50 mM sodium acetate, 100 mM NaCl, 10% $D_2O$, 90% $H_2O$ buffer (pH 5.7). A [U−$^{15}$N,$^2$H]-labeled sample of the L99A mutant of T4 lysozyme (L99A T4L) was generated following established protocols.[5] A 1 mM sample was prepared in 50 mM sodium phosphate buffer, 25 mM NaCl, 2 mM EDTA, 2 mM $NaN_3$, 10% $D_2O$, and 90% $H_2O$ (pH 5.5).

**NMR Spectroscopy.** An $^{15}$N CEST data set[16] was recorded on protein L, 1 °C, 11.7 T (room temperature probehead), using an $^{15}$N $B_1$ field strength of 25 Hz applied for a duration $T$ = 0.5 s; simultaneously a $^1$H composite pulse decoupling field of 2.5 kHz (comprising $90_x240_y90_x$ elements) was employed. A total of 62 2D planes were recorded in steps of 25 Hz with the position of the $^{15}$N $B_1$ field ranging from 103.7 to 133.3 ppm. Each plane was recorded with ($t_{1,max}$, $t_{2,max}$) = (39.5, 63.9 ms), two transients per free induction decay (FID) and an interscan delay of 1.5 s for a net acquisition time of ∼6 min and a total measurement time of 6 h for the complete series. In order to illustrate the influence of proximal protons on $^1H^N$ CEST profiles we acquired an $^1H^N$ CEST data set on protein L, 1 °C, 11.7 T (room temperature probehead), using an $^1H^N$ $B_1$ field strength of 15 Hz for $T$ = 0.5 s. A total of 102 data sets were obtained in steps of 15 Hz with $^1H^N$ offsets ranging from 6.85 to 9.85 ppm. 2D planes were recorded with ($t_{1,max}$, $t_{2,max}$) = (31.4, 64.0 ms), two scans/FID and a repetition delay of 2.0 s for a net acquisition time of ∼6 min/plane and a total collection time of 10.3 h for the complete series.

$^{15}$N CEST data sets were obtained on the A39G FF domain sample, 1 °C, 14.0 T (cryogenically cooled probehead), using an $^{15}$N $B_1$ field strength of 18 Hz ($T$ = 0.5 s). A set of 92 2D planes was obtained in steps of 20 Hz with the position of the $^{15}$N $B_1$ field ranging from 104.9 to 133.6 ppm. Each 2D data set was recorded with ($t_{1,max}$, $t_{2,max}$) = (35.6, 63.9 ms), four scans/FID and a repetition delay of 1.5 s, corresponding to a net acquisition time of about 12 min per plane and 18.1 h for the complete series. In order to determine the $^1H^N$ chemical shift of the minor state, several $^{15}$N-CEST data sets were recorded. These include (i) a series of three experiments with an off-resonance $^1$H CW decoupling field of 924 Hz positioned at 7.5, 8.5, and 9.5 ppm, and applied simultaneously with the weak $^{15}$N $B_1$ field (see Figure S1 for the pulse scheme used), (ii) a fully decoupled ("standard") experiment[16] (using a 3 kHz decoupling field) and (iii) a "coupled" experiment (i.e., no $^1$H decoupling during $T$ whatsoever).

A similar set of $^{15}$N CEST experiments was recorded on the L99A T4L sample, 5 °C, 14.0 T (cryogenically cooled probehead), using an $^{15}$N $B_1$ field strength of 14 Hz applied for $T$ = 0.75 s. A set of 80 2D planes were obtained in steps of 30 Hz with the position of the $^{15}$N $B_1$ field ranging from 98.6 ppm to 137.2 ppm. Acquisition times of ($t_{1,max}$, $t_{2,max}$) = (38.0, 63.9 ms) were used, along with four transients per FID and a relaxation delay between scans of 1.5 s (16 min per plane, total collection time of 21 h). A set of three experiments was run with a weak $^1$H CW decoupling field of 941 Hz centered at 7.5, 8.5, and 9.5 ppm, respectively (applied simultaneously with the weak $^{15}$N $B_1$ field; Figure S1) along with fully $^1H^N$ decoupled (in the CEST $^{15}$N dimension, 3 kHz decoupling field) and fully $^1H^N$ coupled experiments.

Each of the CEST data sets described above was recorded with an additional plane where $T$ was set to 0 to allow for a robust estimate of longitudinal relaxation rates.[16] Calibration of the weak $^{15}$N $B_1$ field applied during $T$ was according to the method of Guenneugues et al.[27]

**Data Analysis.** All NMR data were processed and analyzed using the NMRPipe package[28] with signal intensities ($I$) quantified using the line-shape-fitting module of the software. All planes from the same experiment were fit together, assuming identical lineshapes but varying intensities. All data were analyzed using an in-house-written program, ChemEx (available upon request), with the best-fit model parameters extracted by minimization of the target function

$$\chi^2(\xi) = \sum_i \left( \frac{I_i^{\mathrm{exp}} - I_i^{\mathrm{calc}}(\xi)}{\sigma_i^{\mathrm{exp}}} \right)^2 \tag{1}$$

where the summation is over all the experimental data points $i$, $\sigma_i^{\mathrm{exp}}$ is the estimated uncertainty of the measured peak intensity $I_i^{\mathrm{exp}}$, $I_i^{\mathrm{calc}}(\xi)$ is the calculated peak intensity, and $\xi = (x_1, ..., x_n)$ is the set of adjustable model parameters. Uncertainties in the measured intensities, $\sigma_i^{\mathrm{exp}}$, were estimated on a per profile basis using the intensity scatter in regions of the 1D CEST profile that did not contain any intensity dips. The minimum uncertainty was set to the median uncertainty from all residues.

Signal intensities were estimated by numerically integrating the Bloch-McConnell equations[29] (over the period $T$, see Figure S1) describing the evolution of an isolated scalar coupled $^1H^N$−$^{15}$N spin system exchanging between two states,[30,31] G and E, $G \underset{k_{EG}}{\overset{k_{GE}}{\rightleftarrows}} E$,

$$\frac{\mathrm{d}}{\mathrm{d}t}\mathbf{m}(t) = \mathbf{L}\cdot\mathbf{m}(t) \tag{2}$$

where $\mathbf{m}$ is a 30 × 1 column vector with the first (last) 15 rows containing density elements for state G (E)

$$\begin{aligned}\mathbf{m} = (&H_x^G, H_y^G, H_z^G, N_x^G, N_y^G, N_z^G, 2H_x^GN_z^G, 2H_y^GN_z^G,\\ &2H_z^GN_x^G, 2H_z^GN_y^G, 2H_x^GN_x^G, 2H_x^GN_y^G, 2H_y^GN_x^G,\\ &2H_y^GN_y^G, 2H_z^GN_z^G, H_x^E, ...., 2H_z^EN_z^E)^+\end{aligned} \tag{3}$$

and "+" is the transpose operator. Matrix $\mathbf{L}$ is given by

$$\mathbf{L} = \begin{pmatrix} \mathbf{R_G} & \mathbf{0_{15}} \\ \mathbf{0_{15}} & \mathbf{R_E} \end{pmatrix} + \begin{pmatrix} -k_{GE} & k_{EG} \\ k_{GE} & -k_{EG} \end{pmatrix} \otimes \mathbf{1_{15}} \tag{4}$$

that describes the evolution of the spin system in the presence of chemical exchange with $\mathbf{0_{15}}$ ($\mathbf{1_{15}}$) the 15-dimensional null (identity) matrix. In turn,

$$\mathbf{R_i} = -\begin{pmatrix}
R^i_{Hxy} & \omega^i_H & 0 & 0 & 0 & 0 & \eta^i_{H,xy} & \pi J_{HN} & 0 & 0 & 0 & 0 & 0 & 0 & 0 \\
-\omega^i_H & R^i_{Hxy} & \omega_{1H} & 0 & 0 & 0 & -\pi J_{HN} & \eta^i_{H,xy} & 0 & 0 & 0 & 0 & 0 & 0 & 0 \\
0 & -\omega_{1H} & R^i_{Hz} & 0 & 0 & \sigma^i & 0 & 0 & 0 & 0 & 0 & 0 & 0 & 0 & \eta^i_{H,z} \\
0 & 0 & 0 & R^i_{Nxy} & \omega^i_N & 0 & 0 & 0 & \eta^i_{N,xy} & \pi J_{HN} & 0 & 0 & 0 & 0 & 0 \\
0 & 0 & 0 & -\omega^i_N & R^i_{Nxy} & \omega_{1N} & 0 & 0 & -\pi J_{HN} & \eta^i_{N,xy} & 0 & 0 & 0 & 0 & 0 \\
0 & 0 & \sigma^i & 0 & -\omega_{1N} & R^i_{Nz} & 0 & 0 & 0 & 0 & 0 & 0 & 0 & 0 & \eta^i_{N,z} \\
\eta^i_{H,xy} & \pi J_{HN} & 0 & 0 & 0 & 0 & R^i_{2HxyNz} & \omega^i_H & 0 & 0 & 0 & -\omega_{1N} & 0 & 0 & 0 \\
-\pi J_{HN} & \eta^i_{H,xy} & 0 & 0 & 0 & 0 & -\omega^i_H & R^i_{2HxyNz} & 0 & 0 & 0 & 0 & 0 & -\omega_{1N} & \omega_{1H} \\
0 & 0 & 0 & \eta^i_{N,xy} & \pi J_{HN} & 0 & 0 & 0 & R^i_{2HzNxy} & \omega^i_N & 0 & 0 & -\omega_{1H} & 0 & 0 \\
0 & 0 & 0 & -\pi J_{HN} & \eta^i_{N,xy} & 0 & 0 & 0 & -\omega^i_N & R^i_{2HzNxy} & 0 & 0 & 0 & -\omega_{1H} & \omega_{1N} \\
0 & 0 & 0 & 0 & 0 & 0 & 0 & 0 & 0 & 0 & R^i_{2HxyNxy} & \omega^i_N & \omega^i_H & -\mu^i_{mq} & 0 \\
0 & 0 & 0 & 0 & 0 & 0 & \omega_{1N} & 0 & 0 & 0 & -\omega^i_N & R^i_{2HxyNxy} & \mu^i_{mq} & \omega^i_H & 0 \\
0 & 0 & 0 & 0 & 0 & 0 & 0 & 0 & \omega_{1H} & 0 & -\omega^i_H & \mu^i_{mq} & R^i_{2HxyNxy} & \omega^i_N & 0 \\
0 & 0 & 0 & 0 & 0 & 0 & 0 & \omega_{1N} & 0 & \omega_{1H} & -\mu^i_{mq} & -\omega^i_H & -\omega^i_N & R^i_{2HxyNxy} & 0 \\
0 & 0 & \eta^i_{H,z} & 0 & 0 & \eta^i_{N,z} & 0 & -\omega_{1H} & 0 & -\omega_{1N} & 0 & 0 & 0 & 0 & R^i_{2HzNz}
\end{pmatrix} \tag{5}$$

is the 15 × 15 submatrix that describes the evolution of the density elements of state $i$ ($i \in \{G,E\}$) in the absence of chemical exchange.[30,31] In eq 5, $R^i_{Hxy}$ [$R^i_{Nxy}$] denotes the $^1H^N$ [$^{15}N$] in-phase transverse relaxation rate (in $s^{-1}$), $R^i_{Hz}$ [$R^i_{Nz}$] is the $^1H^N$ [$^{15}N$] longitudinal magnetization relaxation rate (in $s^{-1}$), $R^i_{2HxyNz}$ [$R^i_{2HzNxy}$] is the $^1H^N$ [$^{15}N$] antiphase transverse relaxation rate (in $s^{-1}$), $R^i_{2HxyNxy}$ is the relaxation rate of multiple quantum coherence (in $s^{-1}$), $R^i_{2HzNz}$ is the longitudinal two-spin order relaxation rate (in $s^{-1}$), $\eta^i_{H,xy}$ [$\eta^i_{N,xy}$] is the $^1H^N$ [$^{15}N$] transverse dipole-CSA cross-correlated relaxation rate (in $s^{-1}$), $\eta^i_{H,z}$ [$\eta^i_{N,z}$] is the $^1H^N$ [$^{15}N$] longitudinal dipole-CSA cross-correlated relaxation rate (in $s^{-1}$), $\sigma^i$ is the cross relaxation rate between $^1H^N$ and $^{15}N$ spins (in $s^{-1}$), $\mu^i_{mq}$ is the cross-relaxation rate between the multiple-quantum coherence components (in $s^{-1}$), $\omega^i_H$ [$\omega^i_N$] is the offset frequency (in rad·$s^{-1}$) of the $^1H^N$ [$^{15}N$] resonance of state $i$ from the $^1H^N$ [$^{15}N$] $rf$ carrier ($\omega^G_H$ and $\omega^G_N$ are obtained from ground-state peak positions and are not fitting parameters), $\omega_{1H}$ [$\omega_{1N}$] is the applied $^1H^N$ [$^{15}N$] $rf$ field strength (in rad·$s^{-1}$) and $J_{HN}$ is the $^1H^N$-$^{15}N$ scalar coupling constant (fixed to −93 Hz). We have not introduced additional terms that account for the magnetization at thermal equilibrium because these cancel when the phase cycle (phase $\phi 1$) is taken into account (Figure S1).

The effects of $^{15}N$ $B_1$ field inhomogeneity were included by repeating the calculation with 10 different $B_1$ field values equally spaced within $\pm 2\sigma$ around the mean, where $\sigma$ is the estimated standard deviation of the $B_1$ field distribution (about 10% of $B_1$). The final intensity value was obtained by computing the weighted average of all 10 calculations, using coefficients that assumed a Gaussian profile. Numerical simulations assuming a spherical protein with a tumbling time ranging from 5 to 25 ns showed that $\eta^i_{H,xy}$, $\eta^i_{H,z}$, $\sigma^i$, $\mu^i_{mq}$, and $R^i_{Hz}$ marginally affect 1D $^{15}N$-CEST profiles and were consequently set to 0, 0, 0, 0, and 1 $s^{-1}$, respectively, in all the fits. As the molecule spends only a small amount of time in state $E$, many of the relaxation rates of spins in this state ($R^E_{Hxy}$,$R^E_{Nz}$, $R^E_{2HxyNz}$, $R^E_{2HxyNxy}$, $R^E_{2HzNz}$, $\eta^E_{N,xy}$, $\eta^E_{N,z}$) could not be constrained by the data and were therefore assumed to be equal to the rates of corresponding density elements that are germane for state $G$. To further simplify the fitting procedure, the $^1H^N$ and $^{15}N$ antiphase transverse relaxation rates were estimated using the following relations:[32]

$$R^i_{2HzNxy} = R^i_{Nxy} + R^G_{2HzNz} - R^G_{Nz} \tag{6}$$

$$R^G_{2HxyNz} = R^G_{Hxy} - R^G_{Nz} \tag{7}$$

where $R^G_{Nz}$, $R^G_{Nxy}$, and $R^G_{Hxy}$ are fitting parameters (see below) and $R^G_{2HzNz}$ values were measured in independent experiments.

Parameters included in the fits are (i) $k_{ex}$ ($=k_{GE} + k_{EG}$), (ii) $p_E$ (the fractional population of state $E$), (iii) $\varpi^E_H$ and $\varpi^E_N$ ($^1H$ and $^{15}N$ chemical shifts of residues in state $E$, in ppm), (iv) $R^E_{Nxy}$ ($^{15}N$ transverse relaxation rate of state $E$), (v) $R^G_{Nz}$, $R^G_{Nxy}$, $R^G_{Hxy}$, $R^G_{2HxyNxy}$, $\eta^G_{N,xy}$, and $\eta^G_{N,z}$ (a set of six relaxation rates of spins in state G), (vi) and an initial intensity, $I_0$. It should be noted that $k_{ex}$ and $p_E$ are global fitting parameters, common to all of the residues, while $\varpi^E_H$, $\varpi^E_N$,$R^E_{Nxy}$, $R^G_{Nz}$, $R^G_{Nxy}$, $R^G_{Hxy}$, $R^G_{2HxyNxy}$, $\eta^G_{N,xy}$, and $\eta^G_{N,z}$ are residue-specific. Practically the fit of the experimental data was achieved in two steps: (1) First, only $^{15}N$ CEST profiles recorded with broadband, composite $^1H^N$ decoupling were fit together using a previously described procedure,[16] allowing robust estimation of $k_{ex}$ and $p_E$, along with residue-specific values for $\varpi^E_N$, $R^G_{Nz}$, $R^G_{Nxy}$, and $R^E_{Nxy}$. (2) Data from all five experiments (with full $^1H^N$ decoupling, without $^1H^N$ decoupling, with off-resonance CW $^1H^N$ decoupling at three different offsets) were then combined and fit together assuming $k_{ex}$ and $p_E$ values from the previous step. To make sure that the global minimum of the target function was reached, we first performed a grid


dx.doi.org/10.1021/jp311109u | J. Phys. Chem. B 2012, 116, 14311−14317

search in $\varpi_H^E$ with values sampled every 0.25 ppm along a 5 ppm segment centered around $\varpi_H^G$. A final optimization where $\varpi_H^E$ was allowed to float was then run from the best point on the grid.

## RESULTS AND DISCUSSION

**Main Problem with $^1$H-CEST.** Recently, Fawzi et al.[20] have reported a CEST experiment whereby exchange is probed via the $^{15}$N heteroatom, as opposed to the $^1$H spin. This is an important development because it circumvents a major limitation with $^1$H CEST experiments that had been performed on proteins up to that time, as illustrated in Figure 1. Here we have chosen a small 63 residue protein, protein L, that does not show any evidence of chemical exchange on the millisecond time-scale either by CPMG relaxation dispersion[33] or from $^{15}$N CEST experiments.[16] In Figure 1A a single CEST trace is indicated for Glu

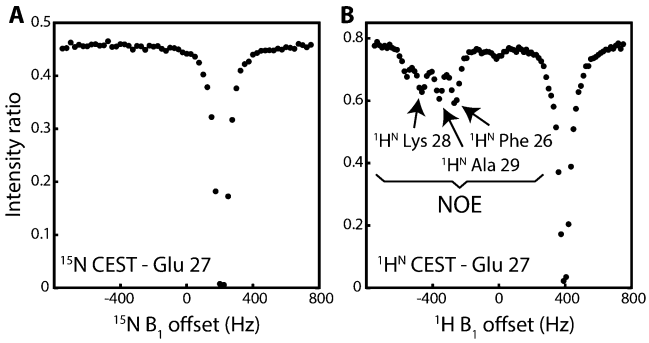


**Figure 1.** $^{15}$N- (A) and $^1$H$^N$- (B) CEST profiles for Glu 27 of protein L, 14.0 T, 1 °C. Only a single dip is observed in the $^{15}$N-CEST trace and for each of the traces from the data set, consistent with the absence of ms time scale chemical exchange in this system. The extra dips in the $^1$H$^N$-CEST derive from NOE magnetization transfer to the $^1$H$^N$ of Glu 27 from proximal protons in the protein (labeled). Experimental details are provided in Materials and Methods.

27 as a function of the offset of a 15 Hz $^{15}$N radio frequency (*rf*) field from the center of the $^{15}$N spectrum (119 ppm), applied for a duration of $T$ = 0.5 ms (see Figure S1 for the pulse scheme). Each point of the trace is proportional to the intensity of the Glu 27 cross peak measured in a 2D experiment, as described previously,[16,20] with magnetization transfer summarized as

$$^1\mathrm{H}^N \rightarrow {}^{15}\mathrm{N}_Z(\mathrm{B}_1, T) \rightarrow {}^1\mathrm{H}^N \quad (8)$$

Equation 8 makes it clear that the $^{15}$N *rf* field is applied during an interval where the magnetization of interest is along $Z$ and, hence, relaxes slowly. $^1$H$^N$ magnetization is decoupled during this interval, as is the case for a "standard" $^{15}$N CEST data set. Typically one additional spectrum is recorded with $T$ = 0 and the intensity ratio of cross peaks in spectra with and without the *rf* element plotted, illustrated in Figure 1A ($Y$ axis).

When the *rf* carrier is placed close to the resonance position of the peak, there is a decrease in its intensity, as expected. The fact that no additional dips in intensity are observed in this case and that similar single dip profiles are recorded for each residue of the protein indicates that additional conformational states cannot be detected. Yet when the corresponding $^1$H$^N$ CEST experiment is recorded many dips beyond that from Glu 27 are observed. These extra dips occur at positions corresponding to resonance frequencies of $^1$H$^N$s that are proximal to the amide proton that is quantified, including Phe 26, Lys 28, and Ala 29. Thus, saturation transfer to the $^1$H$^N$ of Glu 27 from proximal amide protons via the NOE effect generates the extraneous dips in Figure 1B (labeled as NOE). For protein systems undergoing chemical exchange the dips from NOE transfer could well interfere with those of interest from exchange, severely complicating data analysis.

The problem illustrated in Figure 1 for $^1$H$^N$ protons is generic to any $^1$H CEST experiment involving biomolecules such as proteins and a priori it is not clear how to separate NOE and CEST effects. Such a separation is desired, however, because proton chemical shifts of the excited state are often essential for its structural analysis. Unlike $^{15}$N or $^{13}$C chemical shifts that are much more local in nature, $^1$H shifts can be sensitive to the position of aromatic moieties due to ring current effects[34] and therefore they often contain critical long-range information. In what follows, we provide a solution to this problem, illustrated for $^1$H$^N$ chemical shifts, and then validate the approach with a

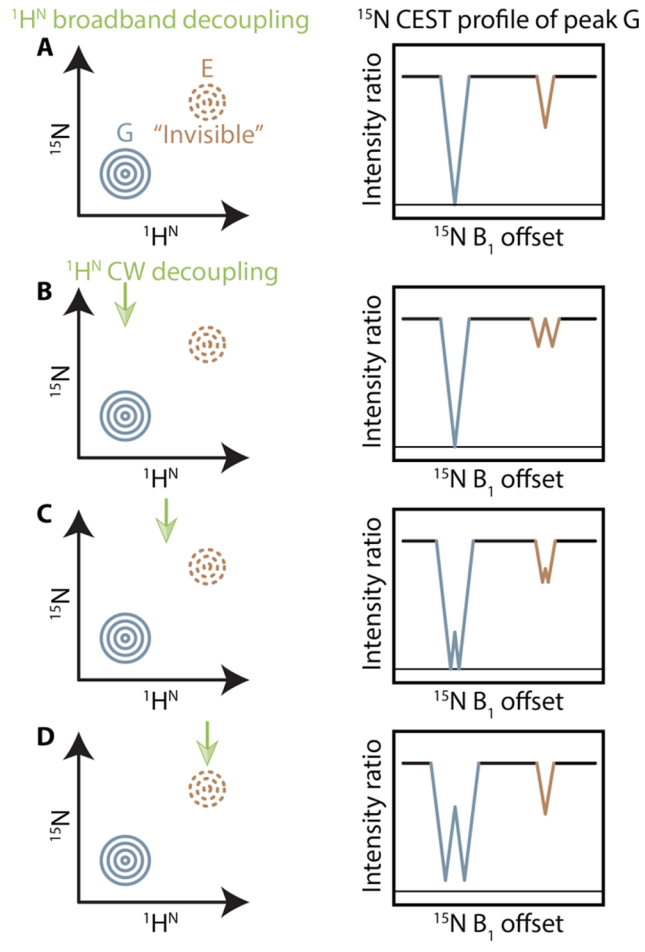


**Figure 2.** Schematic illustrating the proposed method for measuring an excited state $^1$H$^N$ chemical shift indirectly from $^{15}$N-CEST experiments recorded as a function of the position of the $^1$H$^N$ CW decoupling field (B–D). Typically a series of $^{15}$N-CEST data sets are recorded (comprising 60–100 different $^{15}$N B$_1$ offsets; see Materials and Methods) with an ~1 kHz $^1$H$^N$ CW field applied at a set frequency, as illustrated in B–D. In the applications considered here, three separate $^{15}$N-CEST experiments are measured with the $^1$H$^N$ B$_1$ positioned at 7.5, 8.5, and 9.5 ppm. Shown also for reference is the corresponding $^{15}$N-CEST profile recorded with $^1$H$^N$ composite pulse decoupling as described previously[16] (A). Note that the CEST profile is generated by measuring the intensity of peaks from the ground state (G; $Y$ axis) as a function of the offset of a weak $^{15}$N *rf* field ($X$ axis).


dx.doi.org/10.1021/jp311109u | J. Phys. Chem. B 2012, 116, 14311–14317

pair of applications involving folding of an FF domain[4] and conformational exchange of a cavity mutant of T4 lysozyme.[5]

**Solution to the Problem.** Figure 2 shows a schematic of the methodology that has been developed, focusing on a single residue from a two-site exchanging system $G \underset{k_{EG}}{\overset{k_{GE}}{\rightleftarrows}} E$, where G and E correspond to ground and excited states, as described above. The approach builds upon the $^{15}N$ CEST experiment that has been previously shown to be powerful in the analysis of slowly exchanging protein systems.[16,20] In applications to this point, we have used $^{1}H^{N}$ composite pulse decoupling so that $^{15}N$ CEST profiles are obtained with a major dip corresponding to the position of the ground state and a second dip at the $^{15}N$ chemical shift of the corresponding peak derived from the excited state that results from magnetization transfer between the states (Figure 2A). Although the position of this peak (E state) cannot be ascertained from $^{1}H^{N}$-$^{15}N$ correlation maps because of the sparse population of the excited state and its short lifetime, it can be deduced from CEST due to the amplification that is provided by "reading off" intensities of the ground state correlation in a series of data sets where the position of the *rf* carrier is incremented. Note that because $^{15}N$ spins are well isolated and have a low gyromagnetic ratio, *rf* perturbation at the frequency of one spin can only be transferred between exchanging sites so that the NOE effect observed in the $^{1}H$ version is not present.[20] The resonance frequency of the $^{1}H^{N}$ spin must, however, be encoded indirectly and this is accomplished by recording a series of $^{15}N$ CEST data sets with off resonance $^{1}H^{N}$ CW decoupling applied simultaneously with the $^{15}N$ *rf* during $T$ so that partially coupled profiles are obtained. The approach is directly analogous to that used previously where an off resonance decoupling field is applied during an acquisition dimension of an experiment from which chemical shifts of the coupling partner can be obtained through measurement of the residual couplings.[35,36] In the case of interest here, the offset of the $^{1}H^{N}$ *rf* carrier from an amide proton, $\nu_{off}$, is given by the relation[37] $\nu_{off} \approx \nu_{rf}/((J/J_{obs})^2 - 1)^{1/2}$, where $\nu_{rf}$ is the strength of the *rf*, $J$ is the $^{1}H^{N}$-$^{15}N$ one bond scalar coupling, and $J_{obs}$ is the magnitude of the splitting in the presence of the field. The value of the $^{1}H^{N}$ chemical shift is then one of $\nu_{carrier} \pm \nu_{off}$. The two possibilities can be distinguished by recording more than one partially coupled spectrum, as illustrated in Figure 2B–D. In Figure 2B, the $^{1}H^{N}$ *rf* field (denoted in green) is applied at a proton frequency that overlaps with the resonance position of the ground state so that the major dip of the $^{15}N$ CEST profile is decoupled, while the dip at the position of the excited state remains a doublet. In a further $^{15}N$ CEST experiment (Figure 2C) the $^{1}H^{N}$ *rf* field is moved upfield, leading to a CEST profile with partial decoupling of both dips, while yet another experiment with the *rf* field placed close to the E state correlation (Figure 2D) produces a profile with decoupling of the minor state dip. A simultaneous analysis of CEST profiles, Figure 2B–D, using exchange parameters and $^{15}N$ chemical shifts fitted from the standard experiment with composite pulse $^{1}H^{N}$ decoupling[16] (Figure 2A), enables extraction of accurate $^{1}H^{N}$ chemical shifts (see Supporting Information), as is shown below.

**Validation of the Approach.** As a first step to verify the methodology we consider the folding of a small four helix bundle, the FF domain from HYPA/FBP11. We have previously shown by $^{15}N$ CEST that at 1 °C the A39G mutant interconverts between a highly populated native state ($p_N \approx 98.5\%$) and an excited state, corresponding to the unfolded state, with an exchange rate constant, $k_{ex} = k_{NU} + k_{UN} \approx 50\ s^{-1}$.[16] The exchange

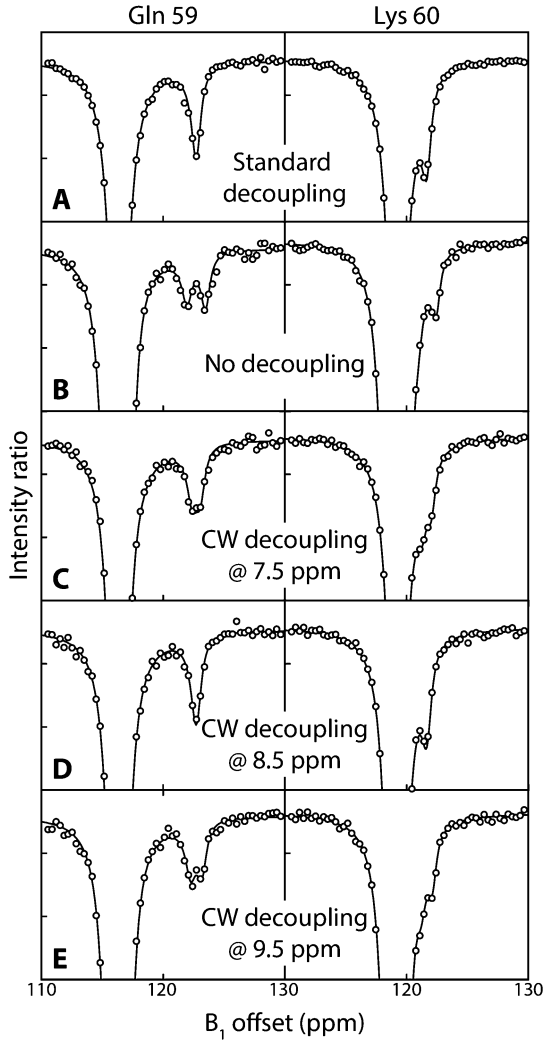


**Figure 3.** $^{15}N$-CEST profiles of residues Gln 59 and Lys 60 of the A39G FF domain, 14.0 T, 1 °C, as a function of the position of the $^{1}H^{N}$ CW decoupling field as indicated. An expansion of the data (circles) is shown so that the dips from the excited state can be more clearly visualized, while those derived from the ground state are off-scale. All dispersion profiles for a given residue are fitted simultaneously to extract accurate values for $^{1}H^{N}$ chemical shifts in the excited state, as described in Materials and Methods. Solid lines are the fits to the experimental data, assuming a two-site exchange process.

reaction is reasonably well approximated as two-state, although from the fitted $^{15}N$ linewidths of the excited conformer it is clear that an additional exchange event is involved that occurs on a time-scale that is over an order of magnitude faster. Figure 3 shows $^{15}N$ CEST profiles for residues Gln 59 and Lys 60 of the A39G FF domain recorded using experiments with broadband composite $^{1}H^{N}$ decoupling during $T$ (A), no decoupling (B) and a 1 kHz $^{1}H^{N}$ CW decoupling field centered at 7.5 (C), 8.5 (D), and 9.5 ppm (E). We have chosen Gln 59 because of its relatively large $^{15}N$ $\Delta\varpi$ value (6.4 ppm) that makes it easy to distinguish the dips from the ground and excited state correlations. A clear doublet is observed for the excited state correlation in the "No Decoupling" case (Figure 3B), while doublets separated by smaller effective couplings are noted when the $^{1}H^{N}$ field is placed at 7.5 ppm (Figure 3C) or 9.5 ppm (Figure 3E). The singlet observed with the *rf* carrier at 8.5 ppm


dx.doi.org/10.1021/jp311109u | J. Phys. Chem. B 2012, 116, 14311–14317

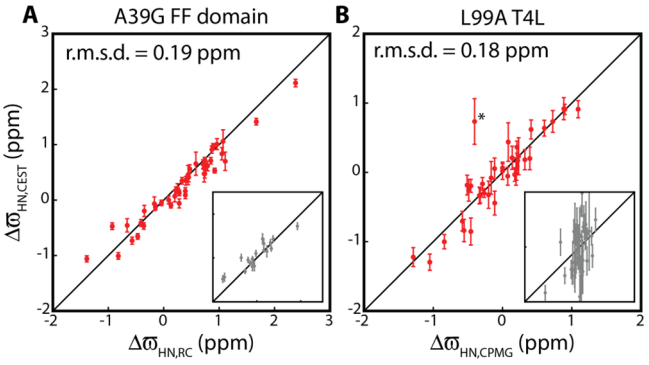


**Figure 4.** (A) Linear correlation plot of $^1H^N$ $\Delta\varpi$ values derived from CEST ($\Delta\varpi_{HN,CEST}$, *Y* axis) vs predicted values for the A39G FF domain, assuming that the excited state can be modeled as a random coil polypeptide ($\Delta\varpi_{HN,RC}$, *X* axis). Main correlation includes those residues where $^{15}N$ $\Delta\varpi$ > 1 ppm; inset for residues where $^{15}N$ $\Delta\varpi$ < 1 ppm. (B) As in (A) but for L99A T4L where the *X* axis ($\Delta\varpi_{HN,CPMG}$) lists amide proton chemical shift differences measured from $^1H^N$ CPMG relaxation dispersion experiments[5] recorded at 25 °C, where $k_{ex}$ is within the window of the dispersion methodology (see text).

makes it clear that the Gln 59 $^1H^N$ chemical shift is nearby. For Lys 60 the $^{15}N$ $\Delta\varpi$ value is smaller (2.5 ppm) so that the major and minor state dips become less resolved, yet an accurate $^1H^N$ chemical shift for the excited state can be extracted for this residue as well from fits of the data (see Supporting Information).

Figure 4A plots the correlation between $^1H^N$ $\Delta\varpi$ values obtained from fits of the CEST data, $\Delta\varpi_{HN,CEST}$ (*Y* axis), versus predicted values where the chemical shifts of the excited state are taken from tabulated values for a random coil polypeptide,[38] $\Delta\varpi_{HN,RC}$ (*X* axis) for those residues where $^{15}N$ $\Delta\varpi$ > 1 ppm (43 of 63 fitted residues). A strong correlation is obtained, confirming that the exchange reaction studied is between native and unfolded states and that the methodology is robust. For the case of Gln 59 and Lys 60 highlighted in Figure 3, $\Delta\varpi_{HN,CEST}$ values of 0.36 ± 0.07 and 0.72 ± 0.05 ppm are fitted that agree well with $\Delta\varpi_{HN,RC}$ = 0.45 and 0.74 ppm. Notably, the root mean squared deviation (rmsd) between $\Delta\varpi$ values, 0.19 ppm, is well under the standard deviation (0.49 ppm) between SPARTA+[39] predicted and experimental $^1H^N$ chemical shifts. This level of error would thus not be problematic for chemical shift based structure determination of excited state conformers based on programs such as CS-Rosetta[14] or Cheshire.[15] Finally, an rmsd of 0.19 ppm must be considered as an upper bound on the experimental error as the tabulated chemical shifts of an unfolded state are of course only an approximation to the true shifts for a particular protein.

The FF domain is small (71 residues) and it is important to establish that the methodology is applicable to larger protein systems as well. As a further example, we have chosen a cavity mutant of T4 lysozyme (164 residues), L99A T4L, that exchanges between a pair of conformers in solution.[5] Experiments have been recorded at 1 °C (correlation time ≈ 25 ns), where $k_{ex}$ = 150 $s^{-1}$, $p_E$ = 1.6%. Here too an excellent correlation is observed between $\Delta\varpi_{HN,CEST}$ values and the corresponding shift differences measured by $^1H^N$ CPMG experiments on the same sample,[5] $\Delta\varpi_{HN,CPMG}$, but at 25 °C, where the exchange rate ($k_{ex}$ = 1350 $s^{-1}$) is more amenable to dispersion experiments, Figure 4B (red,$^{15}N$ $\Delta\varpi$ > 1 ppm).

A limitation with the present methodology is that the measurement of accurate $^1H^N$ chemical shifts of the excited state requires a minimum separation between major and minor state dips in $^{15}N$ CEST profiles, Figure 3. It is of interest, therefore, to establish what the requisite separation might be. The insets to Figure 4A,B show $^1H^N$ $\Delta\varpi$ correlations, as for the main figures, but considering those residues for which $^{15}N$ $\Delta\varpi$ < 1 ppm. In the great majority of cases the errors in extracted chemical shifts increase significantly, with a concomitant decrease in the correlation with the "correct" values. A minimum value for $^{15}N$ chemical shift differences of 1 ppm thus appears to be a requirement of the present method. Notably, in this regard, the largest outlier in Figure 4B (red, denoted by *) is for Arg 137, where $^{15}N$ $\Delta\varpi$ = 1.0 ppm.

Although the CEST method was originally introduced close to 50 years ago and most applications have involved perturbations via $^1H$ *rf* fields, separating dips due to magnetization transfer from chemical exchange or NOE effects has remained problematic. This complicates the use of $^1H$ CEST as a quantitative probe of chemical exchange, at least for many protein applications. Here we provide a simple solution that exploits heteroatom CEST experiments, with the chemical shift of the attached $^1H$ spin provided in an indirect manner. The methodology thus extends the CEST approach to include $^1H$ nuclei whose chemical shifts are important in structural studies of excited protein states.

## ■ ASSOCIATED CONTENT

### Supporting Information

One figure of the pulse scheme used to record data and tables of extracted $^1H^N$ chemical shifts from CEST experiments. This material is available free of charge via the Internet at http://pubs.acs.org.

## ■ AUTHOR INFORMATION

### Corresponding Author

*E-mail: guillaume@pound.med.utoronto.ca (G.B.); kay@pound.med.utoronto.ca (L.E.K.). Tel.:416-978-0741 (L.E.K.). Fax: 416-978-6885 (L.E.K.).

### Notes

The authors declare no competing financial interest.

## ■ ACKNOWLEDGMENTS

This work was supported by grants from the Canadian Institutes of Health Research and the Natural Sciences and Engineering Research Council of Canada. L.E.K. holds a Canada Research Chair in Biochemistry.

## ■ REFERENCES

(1) Karplus, M.; Kuriyan, J. *Proc. Natl. Acad. Sci. U.S.A.* **2005**, *102*, 6679−85.
(2) Palmer, A. G.; Kroenke, C. D.; Loria, J. P. *Methods Enzymol.* **2001**, *339*, 204−238.
(3) Hansen, D. F.; Vallurupalli, P.; Kay, L. E. *J. Biomol. NMR* **2008**, *41*, 113−20.
(4) Korzhnev, D. M.; Religa, T. L.; Banachewicz, W.; Fersht, A. R.; Kay, L. E. *Science* **2010**, *329*, 1312−6.
(5) Bouvignies, G.; Vallurupalli, P.; Hansen, D. F.; Correia, B. E.; Lange, O.; Bah, A.; Vernon, R. M.; Dahlquist, F. W.; Baker, D.; Kay, L. E. *Nature* **2011**, *477*, 111−114.
(6) Neudecker, P.; Robustelli, P.; Cavalli, A.; Walsh, P.; Lundstrom, P.; Zarrine-Afsar, A.; Sharpe, S.; Vendruscolo, M.; Kay, L. E. *Science* **2012**, *336*, 362−6.
(7) Boehr, D. D.; McElheny, D.; Dyson, H. J.; Wright, P. E. *Science* **2006**, *313*, 1638−42.
(8) Fraser, J. S.; Clarkson, M. W.; Degnan, S. C.; Erion, R.; Kern, D.; Alber, T. *Nature* **2009**, *462*, 669−73.

(9) Ishima, R.; Freedberg, D. I.; Wang, Y. X.; Louis, J. M.; Torchia, D. A. *Struct. Fold Des.* **1999**, *7*, 1047−1055.
(10) Nikolova, E. N.; Kim, E.; Wise, A. A.; O'Brien, P. J.; Andricioaei, I.; Al-Hashimi, H. M. *Nature* **2011**, *470*, 498−502.
(11) Kloiber, K.; Spitzer, R.; Tollinger, M.; Konrat, R.; Kreutz, C. *Nucleic Acids Res.* **2011**, *39*, 4340−51.
(12) Carr, H. Y.; Purcell, E. M. *Phys. Rev.* **1954**, *54*, 630−638.
(13) Meiboom, S.; Gill, D. *Rev. Sci. Instrum.* **1958**, *29*, 688−691.
(14) Shen, Y.; Lange, O.; Delaglio, F.; Rossi, P.; Aramini, J. M.; Liu, G.; Eletsky, A.; Wu, Y.; Singarapu, K. K.; Lemak, A.; et al. *Proc. Natl. Acad. Sci. U.S.A.* **2008**, *105*, 4685−90.
(15) Cavalli, A.; Salvatella, X.; Dobson, C. M.; Vendruscolo, M. *Proc. Natl. Acad. Sci. U.S.A.* **2007**, *104*, 9615−20.
(16) Vallurupalli, P.; Bouvignies, G.; Kay, L. E. *J. Am. Chem. Soc.* **2012**, *134*, 8148−61.
(17) Forsen, S.; Hoffman, R. A. *J. Chem. Phys.* **1963**, *39*, 2892−2901.
(18) Cayley, P. J.; Albrand, J. P.; Feeney, J.; Roberts, G. C.; Piper, E. A.; Burgen, A. S. *Biochemistry* **1979**, *18*, 3886−95.
(19) Gupta, R. K.; Redfield, A. G. *Science* **1970**, *169*, 1204−6.
(20) Fawzi, N. L.; Ying, J.; Ghirlando, R.; Torchia, D. A.; Clore, G. M. *Nature* **2011**, *480*, 268−72.
(21) Hyde, E. I.; Birdsall, B.; Roberts, G. C.; Feeney, J.; Burgen, A. S. *Biochemistry* **1980**, *19*, 3738−46.
(22) Ward, K. M.; Aletras, A. H.; Balaban, R. S. *J. Magn. Reson.* **2000**, *143*, 79−87.
(23) Zhou, J. Y.; van Zijl, P. C. M. *Prog. Nucl. Magn. Reson. Spectrosc.* **2006**, *48*, 109−136.
(24) Bouvignies, G.; Kay, L. E. *J. Biomol. NMR* **2012**, *53*, 303−10.
(25) Mittermaier, A.; Kay, L. E. *J. Am. Chem. Soc.* **2001**, *123*, 6892−903.
(26) Jemth, P.; Day, R.; Gianni, S.; Khan, F.; Allen, M.; Daggett, V.; Fersht, A. R. *J. Mol. Biol.* **2005**, *350*, 363−78.
(27) Guenneugues, M.; Berthault, P.; Desvaux, H. *J. Magn. Reson.* **1999**, *136*, 118−126.
(28) Delaglio, F.; Grzesiek, S.; Vuister, G. W.; Zhu, G.; Pfeifer, J.; Bax, A. *J. Biomol. NMR* **1995**, *6*, 277−293.
(29) McConnell, H. M. *J. Chem. Phys.* **1958**, *28*, 430−431.
(30) Allard, P.; Helgstrand, M.; Hard, T. *J. Magn. Reson.* **1998**, *134*, 7−16.
(31) Helgstrand, M.; Hard, T.; Allard, P. *J. Biomol. NMR* **2000**, *18*, 49−63.
(32) Cavanagh, J.; Fairbrother, W. J.; Palmer, A. G.; Skelton, N. J. *Protein NMR Spectroscopy: Principles and Practice*; Academic Press: San Diego, 1996; p 912.
(33) Korzhnev, D. M.; Kloiber, K.; Kanelis, V.; Tugarinov, V.; Kay, L. E. *J. Am. Chem. Soc.* **2004**, *126*, 3964−73.
(34) Wüthrich, K. *NMR of Proteins and Nucleic Acids*; John Wiley & Sons: New York, 1986.
(35) Grace, C. R.; Riek, R. *J. Am. Chem. Soc.* **2003**, *125*, 16104−13.
(36) Fesik, S. W.; Eaton, W. A.; Olejniczak, E. T.; Gampe, R. T. *J. Am. Chem. Soc.* **1990**, *112*, 5370−5371.
(37) Freeman, R. *A Handbook of Nuclear Magnetic Resonance*; John Wiley & Sons: New York, 1988.
(38) Tamiola, K.; Acar, B.; Mulder, F. A. *J. Am. Chem. Soc.* **2010**, *132*, 18000−18003.
(39) Shen, Y.; Bax, A. *J. Biomol. NMR* **2010**, *48*, 13−22.